Optics Communications 291 (2013) 424–434

Contents lists available at SciVerse ScienceDirect

Optics Communications

journal homepage: www.elsevier.com/locate/optcom

Analysis of optical properties in cylindrical dielectric photonic crystal

Chung-An Hu [a], Chien-Jang Wu [b,*], Tzong-Jer Yang [c], Su-Lin Yang [a]

[a] Department of Electrophysics, National Chiao Tung University, Hsinchu 300, Taiwan
[b] Institute of Electro-Optical Science and Technology, National Taiwan Normal University, Taipei 116, Taiwan
[c] Department of Electrical Engineering, Chung Hua University, Hsinchu 300, Taiwan

ARTICLE INFO

Article history:
Received 6 October 2012
Received in revised form
19 November 2012
Accepted 20 November 2012
Available online 5 December 2012

Keywords:
Cylindrical photonic crystal
Transfer matrix method
Wave propagation

ABSTRACT

In this work, theoretical formulas for the *H*-polarization electromagnetic propagation in a cylindrical multilayer structure (CMS) are given. The relationships between two modes, *H*- and *E*-polarization are pointed out. With the derived formulae, we present the numerical results for three model structures such as the single cylindrical interface, the single cylindrical slab, and the cylindrical photonic crystal (CPC). In the single cylindrical interface, it is found that there exists a Brewster starting radius at which a minimum reflectance is attained in *H*-polarization. In the single cylindrical slab, the result illustrates that the reflectance response in the wavelength domain contains the oscillating and nonoscillating regions. As for the CPC, we find the PBG structure at zero azimuthal mode number is very similar to that of planar photonic crystal. The PBG, however, can be strongly influenced by increasing the azimuthal mode number in a CPC.

1. Introduction

The propagation of electromagnetic waves in dielectric stratified structures has been studied for a long time [1,2]. Such an issue has been of much interest to the optical and electromagnetic communities again in 1987 since the concept of the photonic crystals (PCs) was introduced by two pioneering works of Yablonovitch and John [3,4]. Since then a flood of research topics in PCs were triggered in the past two and half decades. At present, research in PCs, which also are called the photonic band gap (PBG) materials, continue to be hot in the communities of photonics, electromagnetics, and material physics.

A simple periodic dielectric multilayer structure known as a one-dimensional (1D) PC is easier to fabricate compared to the two- and three-dimensional PCs. In addition, 1D PCs can be used to explore many fundamental and interesting optical properties, such as the existence of PBGs as well as the feature of omnidirectional mirror [5,6]. In 1D PCs the wave propagation properties can be analytically investigated by the familiar transfer matrix method (TMM) in Cartesian coordinates [1,2,7]. The TMM described in Ref. [7] is generally referred to as the Abeles theory.

In addition to the usual planar 1D PC, wave propagation in a cylindrical multilayer structure (CMS) has also received much attention in recent years [8–17]. A PC with a periodic CMS is called a cylindrical photonic crystal (CPC) or cylindrical Bragg reflector (CBR). The reflection or transmission response of a CPC can be analytically investigated based on another version of TMM. In fact, such cylindrical wave TMM has been developed by Kaliteevski et al. [18]. They developed an elegant TMM in cylindrical coordinates which, in fact, is an analogous version of Abeles theory in Cartesian coordinates. With this cylindrical TMM, the reflection response for the CPC can be studied and then a comparison with planar 1D PC can be made [19]. Moreover, based on the use of such TMM, studies of photonic band structures in metallic and superconducting CPCs have also been available [20,21].

In a CMS, it is known that there will be two possible propagation modes called the *E*-polarization and the *H*-polarization as well [18]. Previous studies [18–21] were all focused in the *E*-polarization only, which is partially because the formulae of the *H*-polarization for the reflection and transmission in a CMS still remain unavailable. The purpose of this paper is thus to give a detailed theoretical description on the wave propagation in a CMS under the condition of *H*-polarization. We shall derive the formulae of reflection and transmission for a CMS. With these formulae, we next give some numerical studies on three model structures, including the single cylindrical interface, the single cylindrical slab, and the CPC. The first structure is similar to Fresnel's formulae in a planar interface between two different media. The study of second structure is reminiscent of the Airy slab problem in optics. The third one, the CPC, is of particular interest in this work because of the current interest. For the purpose of comparative study, all the numerical results of these three structures are given for both *E*- and *H*-polarization.

2. Transfer matrix method in cylindrical system

In this section, we first derive the transfer matrix method (TMM) for the electromagnetic propagation in the CMS as shown

* Corresponding author. Tel.: +886 2 77346724; fax: +886 2 86631954.
E-mail address: jasperwu@ntnu.edu.tw (C.-J. Wu).

0030-4018/$ - see front matter © 2012 Elsevier B.V. All rights reserved.
http://dx.doi.org/10.1016/j.optcom.2012.11.042

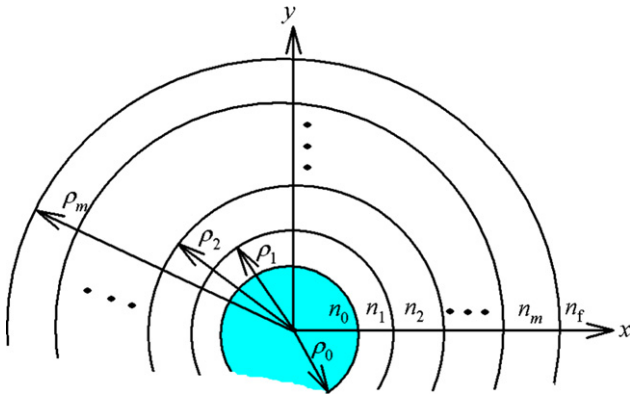

Fig. 1. A portion of CMS, in which the m-layer system/1/2/…/m/ is bounded by the media of refractive indices, n_0 and n_f. The subscript "0" is known as the starting medium, whereas the final medium is indexed by the subscript "f". The dimension in z direction is assumed to be much larger than the dimensions in x and y directions.

in Fig. 1.We assume that the temporal part of all the fields is $\exp(j\omega t)$. In what follows, the SI-unit will be used in this work. For a given layer with permeability $\mu=\mu_r\mu_0$ and permittivity $\varepsilon=\varepsilon_r\varepsilon_0$, Maxwell's curl equations are written as,

$$\nabla\times \mathrm{E}=-j\omega\mu H, \tag{1}$$

$$\nabla\times \mathrm{H}=j\omega\varepsilon \mathrm{E} \tag{2}$$

In cylindrical coordinate, (ρ, ϕ, z), Eq. (1) can be expanded as

$$\frac{1}{\rho}\frac{\partial E_z}{\partial\phi}-\frac{\partial E_\phi}{\partial z}=-j\omega\mu H_\rho, \tag{3a}$$

$$\frac{\partial E_\rho}{\partial z}-\frac{\partial E_z}{\partial\rho}=-j\omega\mu H_\phi, \tag{3b}$$

$$\frac{1}{\rho}\left[\frac{\partial(\rho E_\phi)}{\partial\rho}-\frac{\partial E_\rho}{\partial\phi}\right]=-j\omega\mu H_z, \tag{3c}$$

and expansion of Eq. (2) gives

$$\frac{1}{\rho}\frac{\partial H_z}{\partial\phi}-\frac{\partial H_\phi}{\partial z}=j\omega\varepsilon E_\rho, \tag{4a}$$

$$\frac{\partial H_\rho}{\partial z}-\frac{\partial H_z}{\partial\rho}=j\omega\varepsilon E_\phi, \tag{4b}$$

$$\frac{1}{\rho}\left[\frac{\partial(\rho H_\phi)}{\partial\rho}-\frac{\partial H_\rho}{\partial\phi}\right]=j\omega\varepsilon E_z \tag{4c}$$

Let us first consider the propagation of cylindrical wave diverging from or converging to the axis of symmetry $\rho=0$ (z axis). In this case, the derivatives of the fields with respect to z can be omitted and hence Eq. (3) can be reduced to

$$\frac{1}{\rho}\frac{\partial E_z}{\partial\phi}=-j\omega\mu H_\rho, \tag{5a}$$

$$\frac{\partial E_z}{\partial\rho}=j\omega\mu H_\phi, \tag{5b}$$

$$\frac{1}{\rho}\left[\frac{\partial(\rho E_\phi)}{\partial\rho}-\frac{\partial E_\rho}{\partial\phi}\right]=-j\omega\mu H_z \tag{5c}$$

Likewise, Eq. (4) can be reduced to

$$\frac{1}{\rho}\frac{\partial H_z}{\partial\phi}=j\omega\varepsilon E_\rho, \tag{6a}$$

$$\frac{\partial H_z}{\partial\rho}=-j\omega\varepsilon E_\phi, \tag{6b}$$

$$\frac{1}{\rho}\left[\frac{\partial(\rho H_\phi)}{\partial\rho}-\frac{\partial H_\rho}{\partial\phi}\right]=j\omega\varepsilon E_z \tag{6c}$$

Solutions for Eqs. (5) and (6) can be classified as two modes. One is called the E-polarization which has three non-zero components, E_z, H_ϕ, and H_ρ. The other is H-polarization having non-zero components H_z, E_ϕ, and E_ρ. The solutions for E-polarization have been available [18]. Thus, in this work, we shall limit to the H-polarization. In this case, with Eqs. (6a) and (6b), Eq. (5c) becomes the governing equation for H_z, namely

$$\frac{\partial}{\partial\rho}\left(\frac{1}{\varepsilon}\rho\frac{\partial H_z}{\partial\rho}\right)+\frac{1}{\varepsilon}\frac{1}{\rho}\frac{\partial}{\partial\phi}\left(\frac{\partial H_z}{\partial\phi}\right)+\omega^2\mu\rho H_z=0, \tag{7}$$

which can be further expressed as

$$\rho\frac{\partial}{\partial\rho}\left(\rho\frac{\partial H_z}{\partial\rho}\right)-\rho^2\frac{1}{\varepsilon}\frac{\partial\varepsilon}{\partial\rho}\frac{\partial H_z}{\partial\rho}+\frac{\partial}{\partial\phi}\left(\frac{\partial H_z}{\partial\phi}\right)+\omega^2\mu\varepsilon\rho^2H_z=0 \tag{8}$$

For E-polarization, the above differential equation is read as [18]

$$\rho\frac{\partial}{\partial\rho}\left(\rho\frac{\partial E_z}{\partial\rho}\right)-\rho^2\frac{1}{\mu}\frac{\partial\mu}{\partial\rho}\frac{\partial E_z}{\partial\rho}+\frac{\partial}{\partial\phi}\left(\frac{\partial E_z}{\partial\phi}\right)+\omega^2\mu\varepsilon\rho^2E_z=0 \tag{9}$$

It is seen that the governing differential equations for E-polarization can be obtained from H-polarization by using $H\to E$ and $\varepsilon\to\mu$, and vice versa.

To solve Eq. (8), we let $H_z=V(\rho)\Phi(\phi)$. Then the angular part takes the form,

$$\frac{d^2\Phi}{d\phi^2}+m^2\Phi=0, \tag{10}$$

which has a solution

$$\Phi\sim e^{jm\phi}, \tag{11}$$

where m can be zero, or a positive or negative integer. The radial part of Eq. (8) is,

$$\rho\frac{d}{d\rho}\left(\rho\frac{dV}{d\rho}\right)-\rho^2\frac{1}{\varepsilon}\frac{d\varepsilon}{d\rho}\frac{dV}{d\rho}+\omega^2\mu\varepsilon\rho^2V-m^2V=0 \tag{12}$$

If the permittivity is homogeneous, $\partial\varepsilon/\partial\rho=0$, Eq. (12) reduces to

$$\rho\frac{d}{d\rho}\left(\rho\frac{dV}{d\rho}\right)+\left(k^2\rho^2-m^2\right)V=0, \tag{13}$$

which is a standard Bessel's equation with a solution expressible as,

$$V(\rho)=AJ_m(k\rho)+BY_m(k\rho), \tag{14}$$

where J_m is a Bessel function, Y_m is a Neumann function and A, B are constants. Here,

$$k=\frac{\omega}{c}n \tag{15}$$

is the wave number in medium where c is the speed of light in free space and n is the refractive index of medium. Based on Eqs. (11) and (14), the magnetic field can be written as

$$H_z(\rho,\phi)=V(\rho)e^{jm\phi}=[AJ_m(k\rho)+BY_m(k\rho)]e^{jm\phi} \tag{16}$$

For the non-zero electric fields, Eq. (6a) leads to

$$E_\rho=\frac{m}{\omega\varepsilon}\frac{V(\rho)}{\rho}e^{jm\phi}, \tag{17a}$$

and Eq. (6b) becomes

$$E_\phi=\frac{1}{-j\omega\varepsilon}\frac{\partial V}{\partial\rho}e^{jm\phi}\equiv U(\rho)e^{jm\phi}, \tag{17b}$$

where $U(\rho)$ and $V(\rho)$ are related by

$$\frac{dV}{d\rho} = -j\omega\varepsilon U(\rho) \tag{18}$$

With Eq. (14), the function U can be found to be

$$U(\rho) = jp\left(AJ'_m(k\rho) + BY'_m(k\rho)\right),, \tag{19}$$

where

$$p = \sqrt{\frac{\mu}{\varepsilon}}, \tag{20}$$

is known as the intrinsic impedance of medium ($p = 377\ \Omega$ for free space). We see that V in Eq. (14) and U in Eq. (19) can be used to respectively determine the non-zero electric field components E_ρ and E_ϕ according to Eqs. (17a) and (17b).

In the transfer matrix formalism, it is convenient to set the column vector $(V(\rho),U(\rho))^T$ at a radial position ρ from the above solutions and relate it to the corresponding vector at some other point, say ρ_0 (assuming $\rho_0 < \rho$), by the matrix multiplication [18]:

$$\begin{pmatrix} V(\rho) \\ U(\rho) \end{pmatrix} = \mathrm{M}\begin{pmatrix} V(\rho_0) \\ U(\rho_0) \end{pmatrix} = \begin{pmatrix} M_{11} & M_{12} \\ M_{21} & M_{22} \end{pmatrix}\begin{pmatrix} V(\rho_0) \\ U(\rho_0) \end{pmatrix}, \tag{21}$$

This matrix equation relates the two non-zero electric fields at two distinct radial positions ρ_0 and ρ. The elements of transfer matrix **M** can be found with the help of Eqs. (14) and (19) when the vector $(V(\rho_0),U(\rho_0))$ has been set at a special value of (1,0) or (0,1) [18]. These two choices are similar to those in the Abeles theory in dealing with the planar multilayer structure [7]. With $(V(\rho_0),U(\rho_0)) = (1,0)$, Eq. (21) leads to

$$M_{11} = V(\rho), \quad M_{21} = U(\rho) \tag{22}$$

The explicit expressions for M_{11} and M_{21} can be further obtained as follows. Eqs. (14) and (19) under this special values can be written by

$$AJ_m(k\rho_0) + BY_m(k\rho_0) = 1, \tag{23a}$$

$$AJ'_m(k\rho_0) + BY'_m(k\rho_0) = 0 \tag{23b}$$

It is easy to have

$$A = \frac{Y'_m(k\rho_0)}{2/(\pi k\rho_0)}, \quad B = -\frac{J'_m(k\rho_0)}{2/(\pi k\rho_0)}. \tag{24}$$

Therefore, M_{11} and M_{21}, can be expressed as

$$M_{11} = V(\rho) = \frac{\pi}{2}k\rho_0\left[Y'_m(k\rho_0)J_m(k\rho) - J'_m(k\rho_0)Y_m(k\rho)\right], \tag{25}$$

$$M_{21} = U(\rho) = j\frac{\pi}{2}k\rho_0 p\left[Y'_m(k\rho_0)J'_m(k\rho) - J'_m(k\rho_0)Y'_m(k\rho)\right]. \tag{26}$$

Similarly, with $(V(\rho_0),U(\rho_0)) = (0,1)$, we have

$$M_{12} = V(\rho), \quad M_{22} = U(\rho) \tag{27}$$

Again, from Eqs. (14) and (19), we can solve for A and B, namely

$$A = \frac{j}{p}\frac{Y_m(k\rho_0)}{2/(\pi k\rho_0)}, \quad B = \frac{-j}{p}\frac{J_m(k\rho_0)}{2/(\pi k\rho_0)} \tag{28}$$

The other two matrix elements are thus given by

$$M_{22} = U(\rho) = \frac{\pi}{2}k\rho_0\left[J_m(k\rho_0)Y'_m(k\rho) - Y_m(k\rho_0)J'_m(k\rho)\right], \tag{29}$$

$$M_{12} = V(\rho) = -j\frac{\pi}{2}\frac{k}{p}\rho_0\left[J_m(k\rho_0)Y_m(k\rho) - Y_m(k\rho_0)J_m(k\rho)\right], \tag{30}$$

In the case of E-polarization, the matrix elements are of the same form as, (25), (26), (29), and (30), but with a replacement of$p = \sqrt{\varepsilon/\mu}$ [18].

Finally, it is worth knowing the determinant of the transfer matrix **M**. With Eqs. (25), (26), (29), and (30), it is direct to get the determinant, namely

$$\det\mathrm{M} = M_{11}M_{22} - M_{12}M_{21} = \frac{\rho_0}{\rho} \tag{31}$$

In obtaining the above result, the following identity has been used,

$$J_m(k\rho_0)Y'_m(k\rho_0) - J'_m(k\rho_0)Y_m(k\rho_0) = \frac{2}{\pi k\rho} \tag{32}$$

It is noted that the determinant is simply equal to the ratio of the initial and final radii. Based on Eq. (21), we arrive at the conclusion that the transfer matrix for a region containing two or more different layers is simply the product of the transfer matrices that correspond to all layers. Furthermore, Eq. (31) reveals that the determinant of the total transfer matrix for a CMS is given by the ratio of its internal and external radii.

3. Propagation waves as basic functions

As shown in previous section, we have known that the field solution for the cylindrical wave can be made of the radial and angular parts. The radial part is described by the Bessel function J_m as well as the Neumann function Y_m. However, for the problem of wave propagation, it is convenient to express the field solution as the sum of two contrary propagating waves, i.e., a superposition of ingoing (converging) and outgoing (diverging) waves. These two waves are generally represented by two Hankel functions. For H-polarization, the magnetic and electric fields of outgoing cylindrical wave take the form

$$H_z{}^+ = AH_m^{(2)}(k\rho)\exp(jm\phi), \tag{33}$$

$$E_\phi{}^+ = jpAH_m^{(2)\prime}(k\rho)\exp(jm\phi), \tag{34}$$

where $H_m^{(2)}$ is the Hankel function of the second kind. On the other hand, the ingoing wave is the Hankel function of the first kind, namely

$$H_z{}^- = BH_m^{(1)}(k\rho)\exp(jm\phi) \tag{35}$$

$$E_\phi{}^- = jpBH_m^{(1)\prime}(k\rho)\exp(jm\phi), \tag{36}$$

For a field with azimuthal variation specified by m, the total field of both H_z and E_ϕ can be written as

$$H_z = H_z{}^+ + H_z{}^-, \tag{37}$$

and

$$E_\phi = E_\phi{}^+ + E_\phi{}^- = jpC_m^{(2)}H_z{}^+ + jpC_m^{(1)}H_z{}^-, \tag{38}$$

where

$$C_m^{(1,2)} = H_m^{(1,2)\prime}(k\rho)/H_m^{(1,2)}(k\rho) \tag{39}$$

In order to refer to the layer where the field exists, we introduce the layer label as a second subscript on the coefficient $C_m^{(1,2)}$, and as a subscript of the wavevector k, namely

$$C_{ml}^{(1,2)} = H_m^{(1,2)\prime}(k_l\rho)/H_m^{(1,2)}(k_l\rho), \tag{40}$$

For a layer, say l.

Next, we would like to relate the magnetic fields at the two boundaries for a single layer. The relationship can be described by a matrix **P** which plays the similar role as the *propagation matrix* in a standard TMM in usual planar geometry [2]. This matrix can be constructed as follows. From Eq. (33), the outgoing magnetic

field is rewritten by

$$H_z^+(\rho)=\frac{H_m^{(2)}(k\rho)}{H_m^{(2)}(k\rho_0)}AH_m^{(2)}(k\rho_0)\exp(jm\phi)=\frac{H_m^{(1)}(k\rho)}{H_m^{(1)}(k\rho_0)}H_z^+(\rho_0), \tag{41}$$

And the ingoing magnetic field is expressed as

$$H_z^-(\rho)=\frac{H_m^{(1)}(k\rho)}{H_m^{(1)}(k\rho_0)}BH_m^{(1)}(k\rho_0)\exp(jm\phi)=\frac{H_m^{(1)}(k\rho)}{H_m^{(1)}(k\rho_0)}H_z^-(\rho_0) \tag{42}$$

Eqs. (41) and (42) can be combined as a matrix equation, namely

$$\begin{pmatrix}H_z^+(\rho)\\H_z^-(\rho)\end{pmatrix}=\mathrm{P}\begin{pmatrix}H_z^+(\rho_0)\\H_z^-(\rho_0)\end{pmatrix}, \tag{43}$$

where the propagation matrix is diagonal and given by

$$\mathrm{P}=\begin{pmatrix}\frac{H_m^{(2)}(k\rho)}{H_m^{(2)}(k\rho_0)} & 0\\ 0 & \frac{H_m^{(1)}(k\rho)}{H_m^{(1)}(k\rho_0)}\end{pmatrix} \tag{44}$$

This matrix converts the magnetic field at inner boundary $\rho=\rho_0$ to a point of $\rho=\rho$ inside the layer. It should be mentioned that this matrix **P** is exactly the same as that for the *E*-polarization.

In the usual planar TMM, there is another important matrix called the *dynamical matrix* **D** that relates the boundary conditions between two media [2]. Similarly, there also exists a corresponding matrix in the CMS. To derive this, let us consider the interface between two layers. Based on the continuity of the tangential components of the electric and magnetic fields (H_z,E_ϕ), we can express the interface conditions in terms of (H_z^+,H_z^-). To this end, we introduce matrix **D** that can convert the basis (H_z^+,H_z^-) to (H_z,E_ϕ), namely

$$\begin{pmatrix}H_z\\E_\phi\end{pmatrix}=\mathrm{D}\begin{pmatrix}H_z^+\\H_z^-\end{pmatrix}, \tag{45}$$

where **D** is written by

$$\mathrm{D}=\begin{pmatrix}1 & 1\\ jpC_m^{(2)} & jpC_m^{(1)}\end{pmatrix} \tag{46}$$

Eq. (46) can be easily seen from Eqs. (37) and (38). For the *E*-polarization, the **D**-matrix in Eq. (46) still holds with a replacement of $j\to -j$. In addition, for the nonmagnetic medium, $\mu_r=1$, the determinant of **D** is found to be

$$\det\mathrm{D}=-\frac{1}{\varepsilon_r}\sqrt{\frac{\mu_0}{\varepsilon_0}}\frac{4}{\pi K\rho}\frac{1}{H_m^{(2)}(k\rho)H_m^{(1)}(k\rho)}, \tag{47}$$

where $K=\omega/c$ is the wave number of free space and, in arriving at Eq. (47), we have used the following Wronskian

$$W\left[H_\nu^{(1)}(z),H_\nu^{(2)}(z)\right]=H_\nu^{(1)}(z)H_\nu^{(2)\prime}(z)-H_\nu^{(1)\prime}(z)H_\nu^{(2)}(z)=-\frac{4j}{\pi z} \tag{48}$$

Also, the inverse of **D** can be calculated to be

$$\mathrm{D}^{-1}=\varepsilon_r\sqrt{\frac{\varepsilon_0}{\mu_0}}\frac{\pi}{4}K\rho H_m^{(2)}(k\rho)H_m^{(1)}(k\rho)\begin{pmatrix}-jpC_m^{(1)} & 1\\ jpC_m^{(2)} & -1\end{pmatrix} \tag{49}$$

Next, from Eq. (45) together with the condition of continuity of the tangential field components at the interface of two layers labeled 1 and 2, we have

$$\mathrm{D}_1\begin{pmatrix}H_{z1}^+\\H_{z1}^-\end{pmatrix}=\mathrm{D}_2\begin{pmatrix}H_{z2}^+\\H_{z2}^-\end{pmatrix} \tag{50}$$

Eq. (50) can be rewritten by

$$\begin{pmatrix}H_{z2}^+\\H_{z2}^-\end{pmatrix}=\mathrm{D}_2{}^{-1}\mathrm{D}_1\begin{pmatrix}H_{z1}^+\\H_{z1}^-\end{pmatrix}=\mathrm{D}_{21}\begin{pmatrix}H_{z1}^+\\H_{z1}^-\end{pmatrix}=\begin{pmatrix}d_{11} & d_{12}\\ d_{21} & d_{22}\end{pmatrix}\begin{pmatrix}H_{z1}^+\\H_{z1}^-\end{pmatrix} \tag{51}$$

The matrix $\mathrm{D}_{21}=\mathrm{D}_2{}^{-1}\mathrm{D}_1$ is regarded as *transmission matrix* that links the amplitudes of the waves on the two sides of the interface. With Eqs. (46) and (49), the matrix elements of D_{21} can be obtained, with the results

$$d_{11}=-j\varepsilon_r\sqrt{\frac{\varepsilon_0}{\mu_0}}\frac{\pi}{4}K\rho H_m^{(2)}(k_2\rho)H_m^{(1)}(k_2\rho)\left[p_2C_m^{(1)}-p_1C_m^{(2)}\right], \tag{52a}$$

$$d_{21}=-j\varepsilon_r\sqrt{\frac{\varepsilon_0}{\mu_0}}\frac{\pi}{4}K\rho H_m^{(2)}(k_2\rho)H_m^{(1)}(k_2\rho)\left[p_1C_m^{(2)}-p_2C_m^{(2)}\right],, \tag{52b}$$

$$d_{12}=-j\varepsilon_r\sqrt{\frac{\varepsilon_0}{\mu_0}}\frac{\pi}{4}K\rho H_m^{(2)}(k_2\rho)H_m^{(1)}(k_2\rho)\left[p_2C_m^{(1)}-p_1C_m^{(1)}\right], \tag{52b}$$

$$d_{22}=-j\varepsilon_r\sqrt{\frac{\varepsilon_0}{\mu_0}}\frac{\pi}{4}K\rho H_m^{(2)}(k_2\rho)H_m^{(1)}(k_2\rho)\left[p_1C_m^{(1)}-p_2C_m^{(2)}\right] \tag{52d}$$

4. Reflection and transmission in a single cylindrical interface

We are in the position to determine the wave reflection and transmission in a cylindrical interface. These formulae of wave reflection and transmission between two media are analogous to the usual Fresnel's equations in the planar geometry. Let us consider a diverging wave incident from medium 1 on the interface between layers 1 and 2. Based on Eq. (51), it is direct to have the reflection coefficient r_d and the transmission coefficient that should satisfy the following relation,

$$\begin{pmatrix}t_d\\0\end{pmatrix}=\mathrm{D}_{21}\begin{pmatrix}1\\r_d\end{pmatrix} \tag{53}$$

It can be seen from Eq. (53) that r_d and t_d are respectively expressed as

$$r_d=-\frac{d_{21}}{d_{22}}=\frac{p_2C_{m2}^{(2)}-p_1C_{m1}^{(2)}}{p_1C_{m1}^{(1)}-p_2C_{m2}^{(2)}}, \tag{54}$$

and

$$t_d=d_{11}+d_{12}r_d=d_{11}-d_{12}\frac{d_{21}}{d_{22}}=\frac{\det\mathrm{D}_{21}}{d_{22}} \tag{55}$$

Here, the determinant of D_{21} can be calculated from Eqs. (51) and (47), namely

$$\begin{aligned}\det\mathrm{D}_{21}&=\det\mathrm{D}_2{}^{-1}\det\mathrm{D}_1\\&=\varepsilon_r\sqrt{\frac{\varepsilon_0}{\mu_0}}\left[\frac{\pi}{4}K\rho H_m^{(2)}(k_2\rho)H_m^{(1)}(k_2\rho)\right]^2\begin{vmatrix}-jp_2C_{m2}^{(1)} & 1\\ jp_2C_{m2}^{(2)} & -1\end{vmatrix}\\&\cdot\frac{-4}{\pi K\rho}\frac{1}{H_m^{(2)}(k_1\rho)H_m^{(1)}(k_1\rho)}\end{aligned} \tag{56}$$

To simplify Eq. (56), we first consider the fact that

$$\begin{aligned}\mathrm{I}=\mathrm{D}_2\mathrm{D}_2{}^{-1}&=\varepsilon_r\sqrt{\frac{\varepsilon_0}{\mu_0}}\frac{\pi}{4}K\rho H_m^{(2)}(k_2\rho)H_m^{(1)}(k_2\rho)\\&\times\begin{pmatrix}-jp_2C_{m2}^{(1)}+jp_2C_{m2}^{(2)} & 0\\ 0 & -jp_2C_{m_2}^{(1)}+jp_2C_{m_2}^{(2)}\end{pmatrix},\end{aligned}$$

which indicates that

$$\varepsilon_r\sqrt{\frac{\varepsilon_0}{\mu_0}}\frac{\pi}{4}K\rho H_m^{(2)}(k_2\rho)H_m^{(1)}(k_2\rho)\left[-jp_2C_{m2}^{(1)}+jp_2C_{m2}^{(2)}\right]=1 \tag{57}$$

By making use of Eq. (57), Eq. (56) becomes

$$\det D_{21} = \frac{H_m^{(2)}(k_2\rho)H_m^{(1)}(k_2\rho)}{H_m^{(2)}(k_1\rho)H_m^{(1)}(k_1\rho)} \tag{58}$$

Therefore, the transmission coefficient in Eq. (55) can be cast as

$$t_d = \frac{-j4\varepsilon_r^{-1}\sqrt{\mu_0/\varepsilon_0}}{\pi K\rho H_m^{(2)}(k_1\rho)H_m^{(1)}(k_1\rho)\left[p_2C_{m2}^{(2)} - p_1C_{m1}^{(1)}\right]} \tag{59}$$

Eqs. (54) and (59) are the reflection coefficient and transmission coefficient for the diverging wave. Similarly, if we are interested in the converging wave, expressions for reflection coefficient and transmission coefficient can be obtained, with the results

$$r_c = \frac{p_2C_{m2}^{(1)} - p_1C_{m2}^{(1)}}{p_1C_{m1}^{(1)} - p_2C_{m2}^{(2)}}, \tag{60}$$

$$t_c = \frac{-j4\varepsilon_r^{-1}\sqrt{\mu_0/\varepsilon_0}}{\pi K\rho H_m^{(2)}(k_2\rho)H_m^{(1)}(k_2\rho)\left[p_2C_{m2}^{(2)} - p_1C_{m1}^{(1)}\right]} \tag{61}$$

The reflection coefficient and transmission coefficient described in Eqs. (54), (59), and (60), (61) are the Fresnel-like equations in the cylindrical interface between the media 1 and 2. In addition, these four equations are of the same forms as in the *E*-polarization with different definitions in parameter *p*.

5. Reflection and transmission in a cylindrical slab

Let us now focus on the wave reflection and transmission in a single cylindrical slab. This issue is reminiscent of the case of Airy formula for a single slab in the usual planar geometry. Fig. 2 depicts a single layer of index n_1 and of thickness $\rho_1-\rho_0$. Here, for the purpose of illustration, we have intentionally plotted the straight line to represent the cylindrical interface. Reflection coefficient r and transmission coefficient t can be derived as follows. Let us denote the transmission and reflection coefficients at the second interface $\rho = \rho_1$ as t_{1d} and r_{1d}. In addition, the coefficients of the first interface $\rho=\rho_0$ as t_{0d}, t_{0c}, r_{0d}, and r_{0c}, the subscripts d and c mean the outgoing and incoming waves, respectively. The explicitly expression for r and t are given by

$$r = \frac{r_{0d} + (t_{0c}t_{0d} - r_{0c}r_{1d})r_{1d}\Theta}{1 - r_{0c}r_{1d}\Theta}, \tag{62}$$

$$t = \frac{t_{0d}t_{1d}}{1 - r_{0c}r_{1d}\Theta}\frac{H_m^{(2)}(k_1\rho_1)}{H_m^{(2)}(k_1\rho_0)}, \tag{63}$$

where

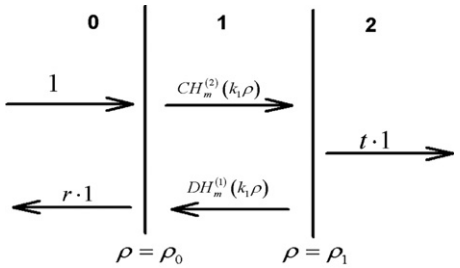

Fig. 2. A circular single layer of index n_1 and of thickness $\rho_1-\rho_0$ bounded by media 0 and 2. Here, the curved interfaces are intentionally plotted as straight lines for convenience of illustration.

$$\Theta = \frac{H_m^{(1)}(k_1\rho_1)}{H_m^{(2)}(k_1\rho_1)}\frac{H_m^{(2)}(k_1\rho_1)}{H_m^{(1)}(k_1\rho_1)}, \tag{64}$$

and k_1 is the wave vector in layer 1.

The derivation of Eqs. (62)–(64) can be described as follows. Referring to Fig. 2, at the first boundary $\rho=\rho_0$, we have

$$CH_m^{(2)}(k_1\rho_0) = 1\cdot t_{0d} + r_{0c}\cdot DH_m^{(1)}(k_1\rho_0), \tag{65}$$

$$1\cdot r = 1\cdot r_{0d} + t_{0c}\cdot DH_m^{(1)}(k_1\rho_0), \tag{66}$$

Similarly, at the second boundary $\rho=\rho_1$, we have

$$t\cdot 1 = t_{1d}\cdot CH_m^{(2)}(k_1\rho_1), \tag{67}$$

$$DH_m^{(1)}(k_1\rho_1) = r_{1d}\cdot CH_m^{(2)}(k_1\rho_1) \tag{68}$$

Eliminating D from Eqs. (65) and (68) leads to

$$C\left[H_m^{(2)}(k_1\rho_0) - r_{1d}\frac{H_m^{(2)}(k_1\rho_1)}{H_m^{(1)}(k_1\rho_1)}r_{0c}H_m^{(1)}(k_1\rho_0)\right] = t_{0d} \tag{69}$$

Again, eliminating D from Eqs. (66) and (68) gives

$$r - r_{0d} = Cr_{1d}\frac{H_m^{(2)}(k_1\rho_1)}{H_m^{(1)}(k_1\rho_1)}t_{0c}H_m^{(1)}(k_1\rho_0) \tag{70}$$

From Eqs. (69) and (70), it is direct to have the reflection coefficient given in Eq. (62). Similarly, with Eqs. (67) and (69), we can arrive at the result of transmission coefficient given in Eq. (63). In addition, Eqs. (62)–(64) are of the same from as those in the *E*-polarization.

6. Reflection and transmission in cylindrical multilayer structure

We now turn attention to the main issue of this work, that is, the wave propagation in the CMS as depicted in Fig. 1. We would like to derive the analytical expressions for reflection and transmission coefficients. Using these formulae, we shall examine the wave properties in a periodic cylindrical multilayer structure, which is also known as a circular photonic crystal (CPC) or a circular Bragg reflector (CBR).

Referring to Fig. 1, an outgoing wave is incident on the interface, $\rho=\rho_0$, between 0 and 1, and then propagates into the final medium f, which is assumed to extend from $\rho=\rho_f$ to $\rho=\infty$. The amplitudes of the magnetic field and electric fields at ρ_0 and ρ_f can be written in terms of the amplitude reflection and transmission coefficients r_d and t_d together with the transfer matrix **M** defined in Eq. (21), with the results

$$\begin{pmatrix} 1+r_d \\ jp_0C_{m0}^{(2)} + jp_0C_{m0}^{(1)}r_d \end{pmatrix} = \mathrm{M}^{-1}\begin{pmatrix} t_d \\ jp_fC_{mf}^{(2)}t_d \end{pmatrix} \tag{71}$$

The inverse matrix in the right hand side of Eq. (71) is denoted by

$$\mathrm{M}^{-1} = \begin{pmatrix} M_{11} & M_{12} \\ M_{21} & M_{22} \end{pmatrix}^{-1} = \frac{1}{\det \mathrm{M}}\begin{pmatrix} M_{22} & -M_{12} \\ -M_{21} & M_{11} \end{pmatrix} \equiv \begin{pmatrix} M'_{11} & M'_{12} \\ M'_{21} & M'_{22} \end{pmatrix} \tag{72}$$

Eqs. (71) and (12) gives expressions for reflection coefficient r_d and transmission coefficient t_d can be determined, namely

$$r_d = \frac{\left(M'_{21} - jp_0C_{m0}^{(2)}M'_{11}\right) + jp_fC_{mf}^{(2)}\left(M'_{22} - jp_0C_{m0}^{(2)}M'_{12}\right)}{\left(jp_0C_{m0}^{(1)}M'_{11} - M'_{21}\right) + jp_fC_{mf}^{(2)}\left(jp_0C_{m0}^{(1)}M'_{12} - M'_{22}\right)}, \tag{73}$$

$$t_d = \frac{-4\varepsilon_r^{-1}\sqrt{\mu_0/\varepsilon_0}}{\pi K\rho_0 H_m^{(2)}(k_0\rho_0)H_m^{(1)}(k_0\rho_0)\left[\left(jp_0C_{m0}^{(1)}M'_{11}-M'_{21}\right)+jp_fC_{mf}^{(2)}\left(jp_0C_{m0}^{(1)}M'_{12}-M'_{22}\right)\right]} \tag{74}$$

Eqs. (73) and (74) can be used to analyze the photonic band gap structure in a periodic CMS. Finally, it is worth mentioning that Eqs. (73) and (74) can be reduced to those for the E-polarization with a replacement of $j\to -j$.

7. Numerical results and discussion

In the analysis that follows, we would like to study the reflectance responses for three model structures. The first is a simple geometry of single cylindrical interface. This problem is similar to a single planar interface, from which the reflectance can be calculated by the familiar Fresnel reflection formula. The second geometry is a single cylindrical slab. This issue is reminiscent to the problem of Airy slab in the planar geometry. The third structure we are interested in is the circular photonic crystal (CPC). The photonic band gap structure will be investigated.

a. Reflection properties in a single cylindrical interface
To present the numerical results, we first investigate the reflection properties in a single cylindrical interface that separates two regions of refractive indices n_0 (internal medium) and n_1 (external medium). Unlike in the usual planar interface, the starting radius ρ_0 in Fig. 1 may play an important role in the study of wave properties in a cylindrical system. In the problem of a single cylindrical interface, the starting radius is simply the radius of interface. Fig. 3 depicts the reflectance, $R=|r|^2$, versus the starting radius ρ_0 at different azimuthal mode numbers $m=0$, 1, 2, and 4, respectively. Here, $n_0=1$ and $n_1=3$ are used, and the results of E- and H-polarization are respectively given in the upper and lower panels. For E-polarization, the reflectance at $m=0$ is small. The reflectance first increases with ρ_0 near the region of $\rho_0<0.2\lambda$, and then remains nearly a constant. However, the reflectance is decreasing function of ρ_0 for $m>0$. A quick drop in reflectance can be seen at $m=1$. At $m>1$, the reflectance first is unity and then decreases with the increase in ρ_0. At sufficiently large value of ρ_0, the reflectance at $m>0$ converges to that of $m=0$. The reflectance in the H-polarization is quite different from E-polarization. For $m=0$, it is a decreasing function of ρ_0. However, at $m>0$, the reflectance exhibits a dip, as marked by the arrow. This dip with a minimum in reflectance can be regarded as an effective Brewster effect. The dip radius is thus defined as an effective Brewster radius, which is shifted to a larger value as m increases. In addition, at large radius, $\rho_0 \gg \lambda$, both polarizations have the same behavior in reflectance, that is, they remain nearly a constant and approach the limit of $m=0$. Conclusively, the reflectance for both polarization modes can be significantly changed as a function of the starting radius when $\rho_0<\lambda$.
Fig. 4 shows the E-polarization reflectance at distinct refractive index of the medium 1. The left panel is for $m=0$, whereas the right one is for $m=4$. It can be from the figures that the overall reflectance will be increased as n_1 increases. Such an increase in reflectance can be ascribed to the impedance mismatch as in the case of planar boundary between two media. The same behavior is also seen in H-polarization, as illustrated in Fig. 5. The Brewster radius at $m=4$ has been slightly shifted to the right when n_1 is decreased. It means that the Brewster effect can be controlled by n_1 at a fixed azimuthal mode number.
In Fig. 6, we fix the index ratio n_1/n_0 with different combinations of (n_0,n_1). We see that the overall reflectance has been shifted to the left as the index difference, n_1-n_0, increases. The Brewster dip in the H-polarization is narrowed down and moves toward the shorter radius of ρ_0.

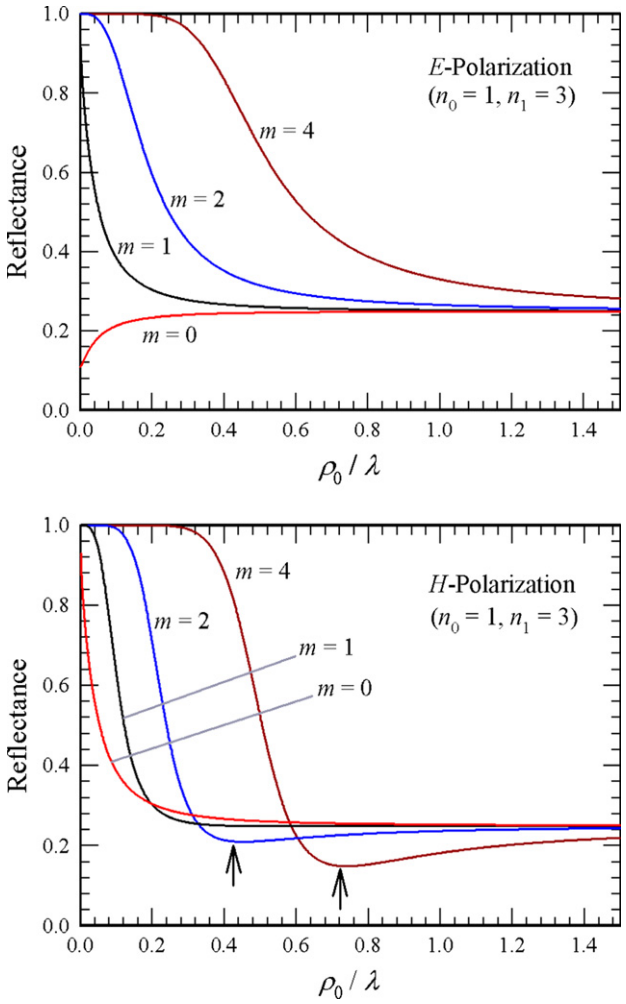

Fig. 3. The calculated reflectance as a function of the radius of the interface ρ_0. Here, ρ_0 is normalized to the wavelength of the incident wave. The left panel is for the E-polarization wave and the H-polarization is shown in the right panel. The refractive indices of inner and outer media are taken to be $n_0=1$ and $n_1=3$, respectively.

b. Reflection properties in a single cylindrical slab
Referring to Fig. 1, we now consider a single cylindrical slab occupying the space of $\rho_0<\rho<\rho_1$. The slab, which is assumed to be immersed in free space ($n_0=1$), has a refractive index of n_1 and a quarter-wavelength thickness of $d=\rho_1-\rho_0=\lambda_0/4n_1$, where λ_0 is called the design wavelength. By taking $n_1=3$, $\rho_0=100$ nm and $\lambda_0=500$ nm, the wavelength-dependent reflectance is depicted in Fig. 7, where different azimuthal mode numbers, $m=0$, 2, and 4 are taken, and the left and right panels are for E- and H-polarization, respectively. It can be seen that the reflectance in the wavelength domain is divided into two regions. The first region located at $\lambda/\rho_0<2$ shows an oscillating behavior. The other nonoscillating region occurs at $\lambda/\rho_0>2$. It means that the starting radius ρ_0 has a strong influence in the reflectance even the thickness of slab is fixed. For both polarizations, at higher m-number, say $m=4$, the wave is completely reflected because of the unity reflectance. If we keep the thickness unchanged and increase the starting radius to a large value of $\rho_0=1000$ nm, the reflectance is shown in Fig. 8. In this case, the oscillating region has been squeezed to a small region of $\lambda/\rho_0<0.4$, i.e., $\lambda<400$ nm. In the

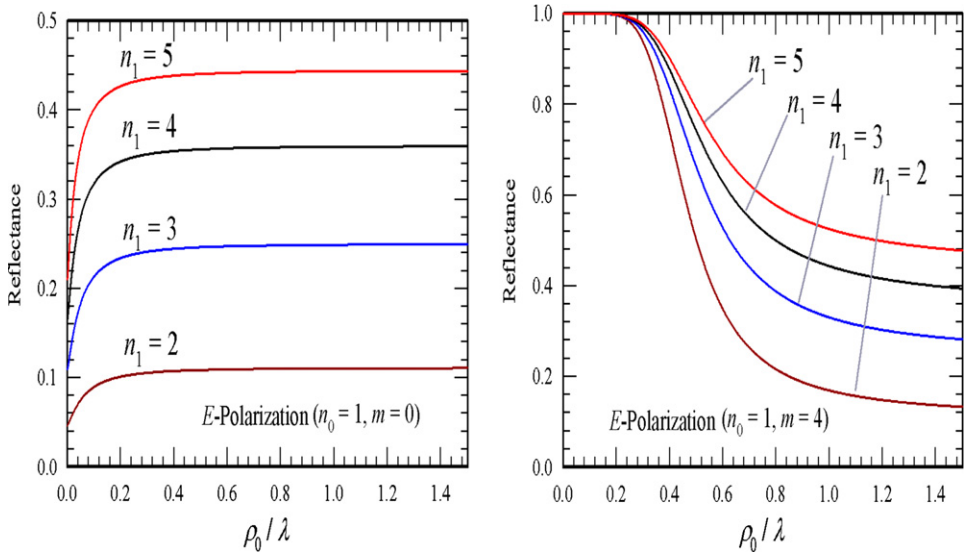

Fig. 4. The calculated E-polarization reflectance as a function of the radius of the interface ρ_0 at $n_0=1$ for different values in $n_1=$ 2, 3, 4, and 5, respectively. The left panel is at $m=0$, whereas the right one is at $m=4$.

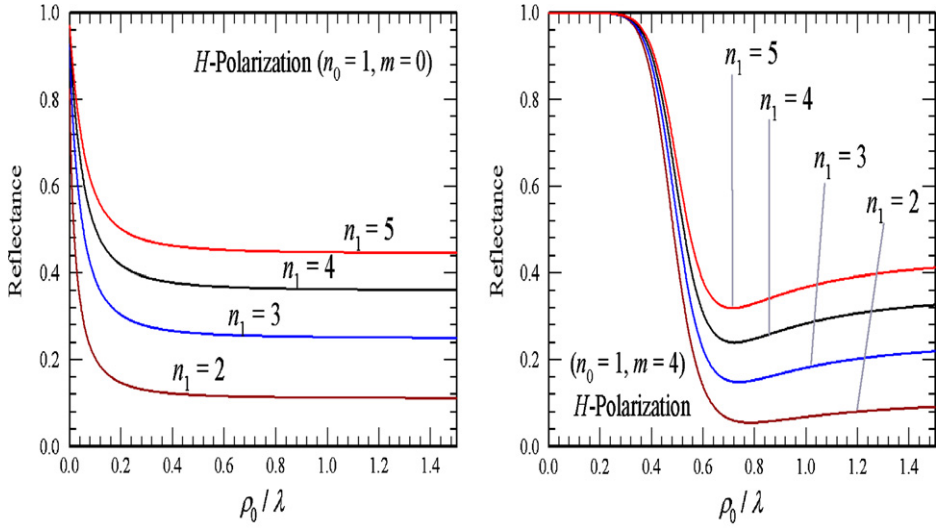

Fig. 5. The calculated H-polarization reflectance as a function of the radius of the interface ρ_0 at $n_0=1$ for different values in n_1. The left panel is at $m=0$, whereas the right one is at $m=4$.

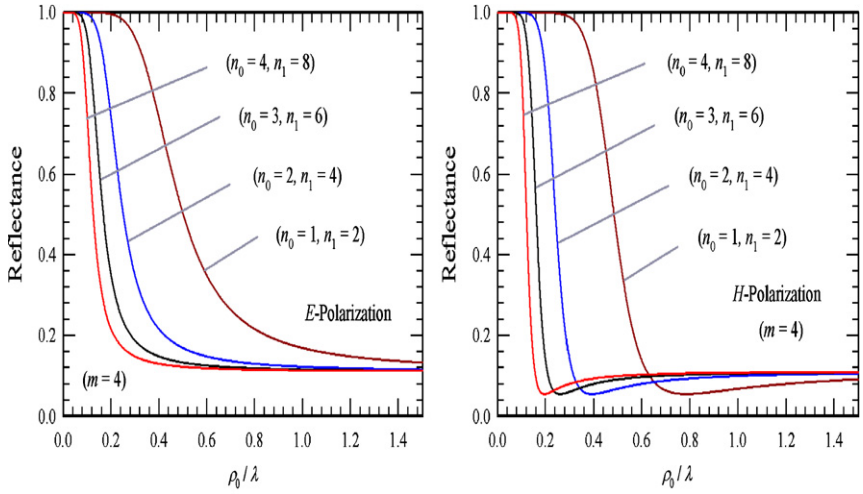

Fig. 6. The calculated E- and H-polarization reflectance as a function of the radius of the interface ρ_0 at $m=4$ for different values in (n_1,n_2).

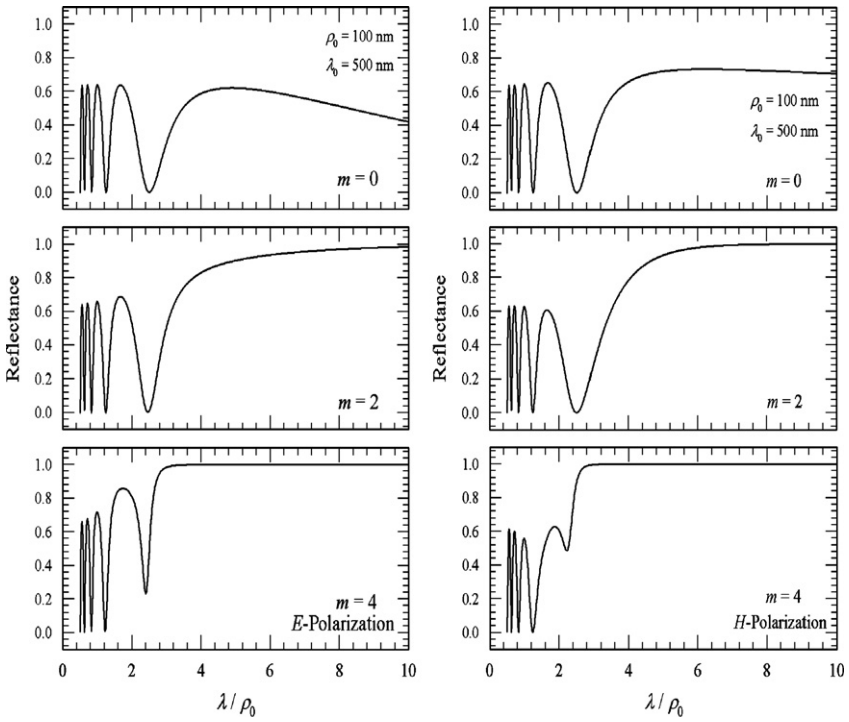

Fig. 7. The calculated *E*- and *H*-polarization reflectance as a function of the wavelength (normalized to the starting radius ρ_0) at $m=0$, 2, and 4, respectively. Here, $\lambda_0=500$ nm and $\rho_0=100$ nm.

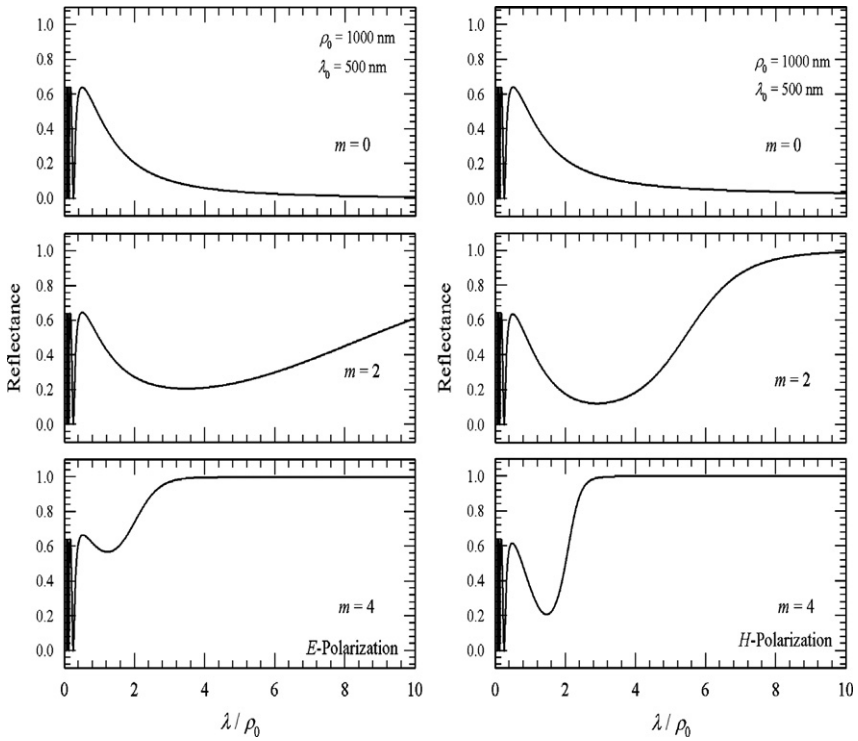

Fig. 8. The calculated *E*- and *H*-polarization reflectance as a function of the wavelength (normalized to the starting radius ρ_0) at $m=0$, 2, and 4, respectively. Here, $\lambda_0=500$ nm and $\rho_0=1000$ nm.

nonoscillating region, the reflectance is influenced substantially at $m=0$, and 2 compared to Fig. 7.

We now investigate the thickness-dependent reflectance. The thickness d can be changed by varying the design wavelength λ_0 when the starting radius ρ_0 is fixed. The reflectance as a function of d is plotted in Fig. 9, where the staring radius is fixed at $\rho_0=100$ nm and the operating wavelength is at $\lambda=500$ nm. Here, the left and right panels are for *E*- and *H*-polarization, respectively. It can be seen from the figure that the reflectance will oscillate as a function of slab thickness at $m=0$, and 2. The reflectance is enhanced at a larger m-value. At $m=4$, the magnitude in reflectance has been highly raised

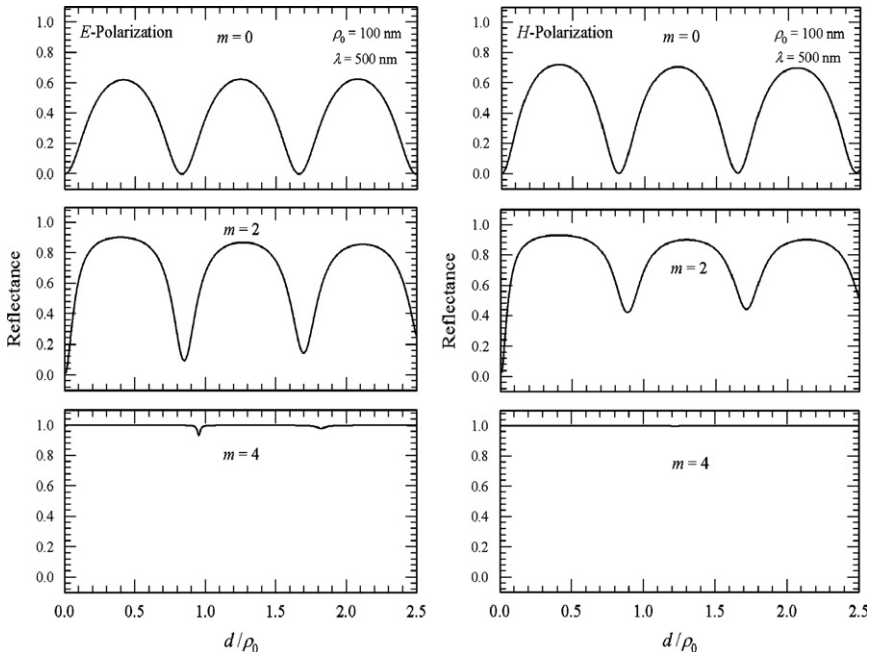

Fig. 9. The calculated E- and H-polarization reflectance as a function of the slab thickness (normalized to the starting radius ρ_0) at $m=0$, 2, and 4, respectively. Here, $\lambda=500$ nm and $\rho_0=100$ nm.

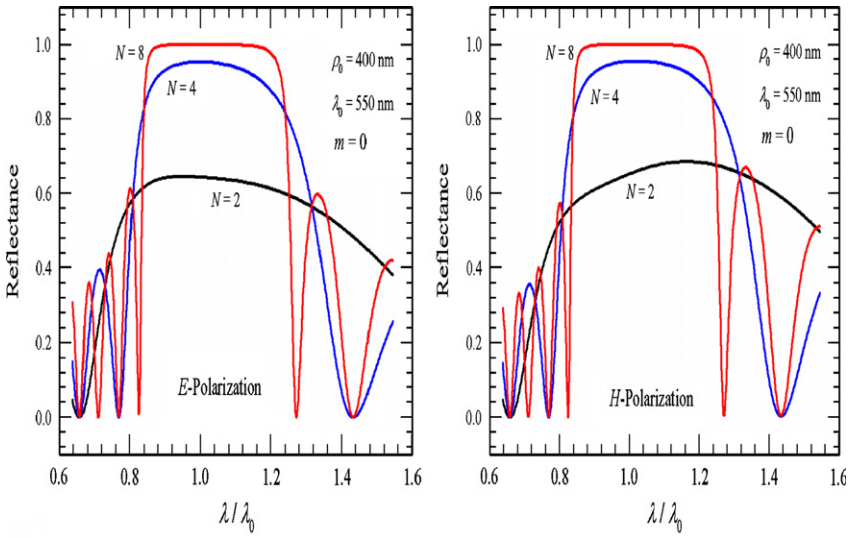

Fig. 10. The calculated E- and H-polarization reflectance as a function of λ/λ_0 at $m=0$ for three different numbers of periods, $N=2$, 4, and 8, respectively. Here, $\lambda_0=$ 550 nm and $\rho_0=400$ nm.

up to unity. The results shown in Fig. 9 are quite different from those of the planar slab, where the reflectance is a decreasing function of slab thickness [2].

c. Reflection properties in a cylindrical photonic crystal

For the third case study, we present the reflectance response for a periodic cylindrical multilayer structure, the cylindrical photonic crystal (CPC). The structure is air/$(H/L)^N$/air, where H and L are the high- and low-index layers, respectively, and N is number of periods. The refractive indices and the thicknesses of H and L are denoted by n_H, n_L, and d_H, d_L, respectively. In the following results, we shall take H as TiO_2 with $n_H=2.40$ and L as MgF_2 with $n_L=1.38$ [22]. In addition, both H and L are taken to be quarter-wavelength layers, i.e., $n_Hd_H=n_Ld_L=\lambda_0/4$. The wavelength-dependent reflectance for E-polarization (left) and H-polarization (right) at $m=0$ is plotted in Fig. 10. Here, $\lambda_0=$ 550 nm and $\rho_0=400$ nm are taken. It is seen that, in the visible region, there is a high-reflectance region (HRR) or photonic band gap (PBG) at a number of periods of $N=8$. For $N=2$ and 4, the PBG cannot be clearly opened up. At $m=0$, there is no obvious difference between the E- and H-polarization. In addition, the reflectance spectra shown here for the CPC are very similar as those in a planar 1D PC [22]. In other words, at $m=0$, the study of PBG structure in a CPC can be effectively replaced by the simple planar 1D PC. At $m=0$, The PBG structure does not related to the geometric curvature in the interfaces.

However, the PBG structure in a CPC can be affected by the nonzero azimuthal mode number. In Figs. 11 and 12, we respectively plot the reflectance spectra of E- and H-polarization at $m>0$ and $N=8$. The PBG structure at $m=0$ in Fig. 10 is now apparently influenced by $m>0$. In E-polarization (Fig. 11), the overall PBG is red-shifted. In addition, the

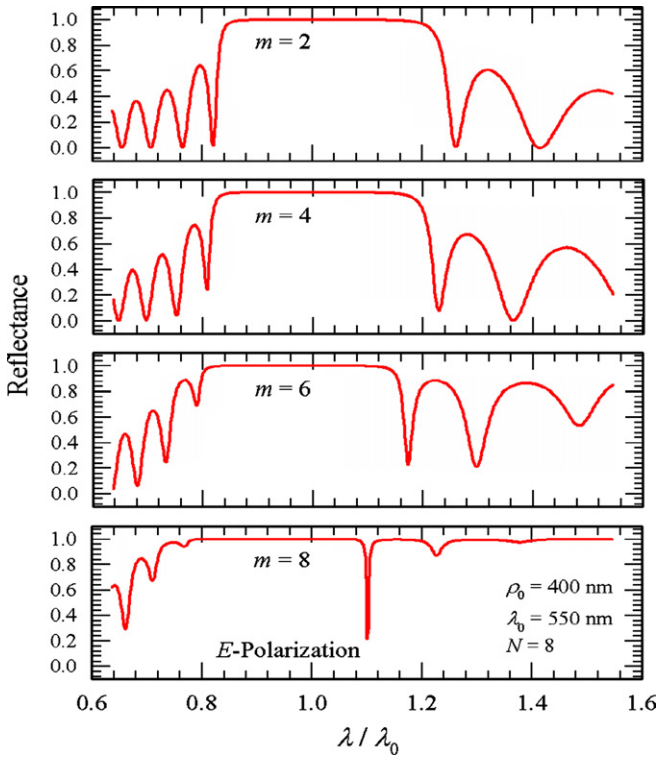

Fig. 11. The calculated *E*-polarization reflectance as a function of the wavelength (normalized to the starting radius λ_0) at $N=8$ for four different azimuthal mode numbers of periods, $m=2$, 4, 6 and 8, respectively. Here, $\lambda_0=$ 550 nm and $\rho_0=400$ nm.

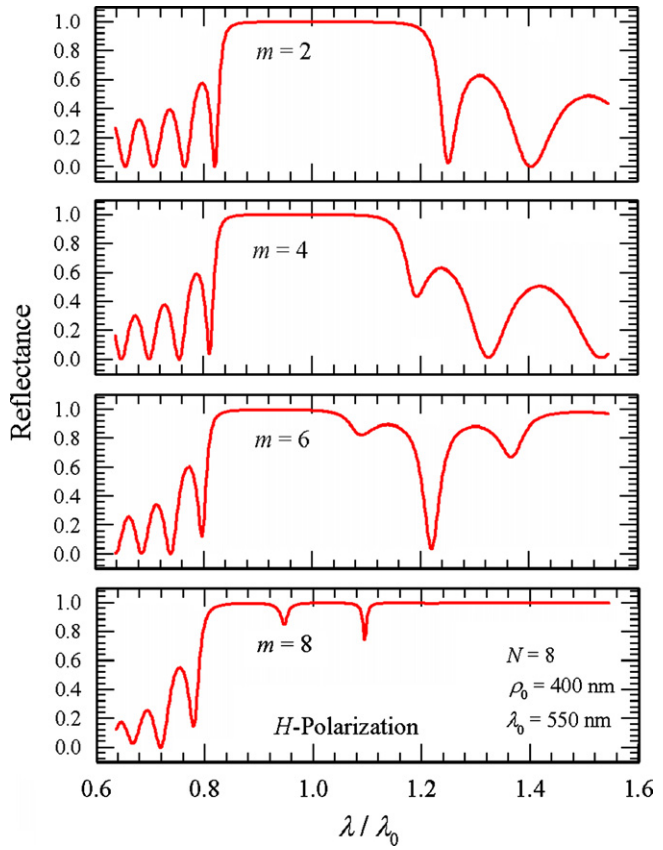

Fig. 12. The calculated *H*-polarization reflectance as a function of the wavelength (normalized to the starting radius λ_0) at $N=8$ for four different azimuthal mode numbers of periods, $m=2$, 4, 6 and 8, respectively. Here, $\lambda_0=$ 550 nm and $\rho_0=400$ nm.

bandwidth of PBG is nearly unchanged as m increases. A pronounced influence in the side lobes (pass bands) can be seen at a large value of m. For example, at $m=8$, the right band edge becomes more sharp and the pass band behind the band edge is highly raised up. In Fig. 12, we can see a salient influence in the PBG structure in *H*-polarization as m increases. The bandwidth of PBG at $m=4$ is smaller than that at $m=2$. At $m=6$, a small dip with reflectance of 0.8 is generated and consequently the size of PBG is reduced. At $m=8$, the right pass band, like in E-polarization, has been lifted up to become a stop band, leading to an enhancement of PBG, except the sharp deep near $\lambda/\lambda_0=1.1$.

Before going into the conclusion, it is worth mentioning the potential applications for the CPC. It can be used to design an annular Bragg reflector (ABR) useful in laser systems [23]. By surrounding a radial defect layer, annular Bragg lasers (or resonators) have been realized and demonstrated [24]. Recently, CPC-based circular-grating microcavity has been available [25]. Moreover, the CPC is an attractive and useful structure in the recent emerging field of transformation optics [26,27].

8. Conclusion

The wave propagation in the cylindrical multilayer structure has been theoretically treated based on the cylindrical wave under *H*-polarization. The transfer matrix method in a cylindrical coordinates has been described. Formulae such as the reflection and transmission coefficients have been given and they strongly related to the azimuthal mode number because of the cylindrical waves. With the derived formulae, we have investigated the reflection responses for three basic cylindrical structures.

In a single cylindrical interface, the reflection responses in both polarizations are strongly dependent on the starting radius as well as the azimuthal mode number. In *H*-polarization, there exists a Brewster radius at which the reflectance attains a minimum. This Brewster radius will increase as the azimuthal mode number increases. On the other hand, it will decrease by increasing the difference in the refractive indices of the two media.

In the single cylindrical slab, the wavelength-dependent reflectance can be divided into the oscillating and nonoscillating regions. The ranges of these two regions are strongly dependent on the starting radius. In the thickness domain, it is found the reflectance has an oscillating behavior. This oscillation is then smeared out at a high value of azimuthal mode number.

In the cylindrical photonic crystal, the PBG structure at $m=0$ is very similar to that of the planar 1D PC. The PBG structure can be significantly changed only at $m>0$. In *E*-polarization, the PBG structure is red-shifted when m is increased. In *H*-polarization, the PBG can be greatly enhanced at a higher m-value.

Acknowledgments

C.-J. Wu acknowledges the financial support from the National Science Council of the Republic of China (Taiwan) under Contract No. NSC-100-2112-M-003-005-MY3 and from the National Taiwan Normal University under NTNU100-D-01.

References

[1] P. Yeh, A. Yariv, C. Hong, Journal of the Optical Society of America 67 (1997) 423.
[2] P. Yeh, Optical Waves in Layered Media, John Wiley & Sons, Singapore, 1991.
[3] E. Yablonovitch, Physical Review Letters 58 (1987) 2059.
[4] S. John, Physical Review Letters 58 (1987) 2486.

[5] Y. Fink, J.N. Winn, S. Fan, C. Chen, J. Michel, J.D. Joannopoulos, L.E. Thomas, Science 282 (1998) 1679.
[6] J.N. Winn, Y. Fink, S. Fan, J.D. Joannopoulos, Optics Letters 23 (1998) 1573.
[7] M. Born, E. Wolf, Principles of Optics, Cambridge, London, 1999.
[8] A. Jebali, D. Erni, S. Gulde, R.F. Mahrt, W. Bachtold, Journal of the Optical Society of America B 24 (2007) 906.
[9] D. Ochoa, R. Houdre, M. Hegems, H. Benisty, T.F. Krauss, C.J.M. Smith, Physical Review B 61 (2000) 4806.
[10] Y.A. Urzhumov, D.R. Smith, Physical Review Letters 105 (2010) 163901.
[11] Z. Liang, J. Li, Optics Express 19 (2011) 16821.
[12] M. Toda, IEEE Journal of Quantum Electronics 26 (1990) 473.
[13] M. Fallahi, F. Chatenoud, I.M. Templeton, M. Dion, C.M. Wu, A. Delage, R. Barber, IEEE Photonics Technology Letters 4 (1992) 1087.
[14] T. Erdogan, O. King, G.W. Wicks, D.G. Hall, E.H. Anderson, M.J. Rooks, Applied Physics Letters 60 (1992) 1921.
[15] W.M. Green, J. Scheuer, G. DeRose, Y. Yariv, Applied Physics Letters 84 (2004) 3669.
[16] J. Scheuer, Y. Yariv, Optics Letters 28 (2003) 1528.
[17] J. Scheuer, J.W.M.J. Green, G. DeRose, Y. Yariv, Optics Letters 29 (2004) 2641.
[18] M.A. Kaliteevski, R.A. Abram, V.V. Nikolaev, G.S. Sokolovski, Journal of Modern Optics 46 (1999) 875.
[19] T.W. Chang, H.-T. Hsu, C.-J. Wu, Journal of Electromagnetic Waves and Applications 25 (2011) 2222.
[20] M.-S. Chen, C.-J. Wu, T.-J. Yang, Optics Communications 285 (2012) 3143.
[21] M.-S. Chen, C.-J. Wu, T.-J. Yang, Solid State Communications 149 (2009) 1888.
[22] F.L. Pedrotti, L.M. Pedrotti, L.S. Pedrotti, Introduction to Optics, Pearson Prentice Education Inc., New Jersey, 2007.
[23] M. Fallahi, F. Chatenoud, I.M. Templeton, M. Dion, C.M. Wu, A. Delage, R. Barber, IEEE Photonics Technology Letters 4 (1992) 1087.
[24] J. Scheuer, W. Green, G. DeRose, Y. Yariv, Proceedings of SPIE 5333 (2004) 183.
[25] A. Jebali, D. Erni, S. Gulde, R.F. Mahrt, W. Batchtold, Journal of the Optical Society of America B 24 (2007) 906.
[26] Z. Liang, J. Li, Optics Express 19 (2011) 16821.
[27] Y.A. Urzhumov, D.R. Smith, Physical Review Letters 105 (2010) 163901.